Comparative mineral mapping of alluvial fans and associated aeolian and lacustrine deposits around the Salton Sea, California using MICA: A new tool for rapid classification of HyspIRI VSWIR imagery

USGS science for a changing world

Bernard E. Hubbard (bhubbard@usgs.gov, 1), John Mars (1), Raymond Kokaly (2), and Donald Hooper (3)

1. US Geological Survey, 12201Sunrise Valley Drive, Reston, VA 20192
2. U.S. Geological Survey, Crustal Geophysics and Geochemistry Science Center, US Geological Survey, Denver, CO, USA
3. Geosciences and Engineering Division, Southwest Research Institute®, San Antonio, TX 78238-5166

Introduction

The wealth of image data that will be produced during the course of the HyspIRI mission creates the need for new software tools and processing algorithms that can be used to rapidly derive land surface material maps from standardized higher level VSWIR (380 – 2500 nm) data products. One potentially useful processing routine is the Material Identification and Characterization Algorithm (MICA) developed at the USGS as a module within the Processing Routines in IDL for Spectroscopic Measurements (PRISM) software. This program can be used as a simple plug-in for the ENVI (ENvironment for Visualizing Images) image processing system. MICA employs continuum removal and linear regression to compare observed spectral absorption features (e.g. such as those in HyspIRI pixel spectra) to those diagnostic of reference materials contained within a spectral library or measured separately in the field or laboratory; as such, it builds on the legacy of the USGS Tetracorder algorithm. PRISM is designed to be "user friendly" and has been applied to mineral detection over large areas such as Afghanistan.

In this study, we show and compare the results of MICA mineral mapping around the Salton Sea area of Southern California, using AVIRIS-classic, AVIRIS-next-generation, Hyperion and AVIRIS-classic convolved to both 30-m and 60-m simulated HyspIRI datasets. Examples of minerals mapped successfully using MICA includes: calcite and aragonite dominating lacustrine deposits left by the receding Lake Cahuilla; montmorillonite, illite and/or muscovite found as coatings on quartz grains in wind-blown aeolian deposits; and variable mineralogy of alluvial fans depending on their source bedrock compositions and surface processes of modification. For example, some alluvial fans are dominated by muscovite, chlorite and/or epidote depending on the amount of unaltered granite relative to mylonitized granite and schists found in bar-n-swale materials. Younger and more active fans tend to be dominated by weathering clays such as montmorillionite, which forms abundant soil crusts after major floods. Montmorillonite often mixes with kaolinite and muscovite in alluvial fans derived from hydrothermally altered source volcanic rocks. Older alluvial fans tend to be dominated by desert varnish coatings containing nanocrystalline forms of hematite, mixed with montmorillonite and/or illite. Additional Fe2+, Fe3+, serpentine minerals, buddingtonite and gypsum were mapped in other bedrock areas, as well as ancient and modern geothermal deposits. We also highlight differences between mineral and vegetation maps caused by variations in the spatial-, spectral- and radiometric-resolution characteristics of the sensor data being input to MICA. Finally, we also assess data quality issues by comparing spectra from these sensors with in situ measurements of our study area collected using an ASD (Analytical Spectral Device) field spectrometer during August 2013 and June 2014.

Salton Sea, Southern California Study Area, Datasets and Methods

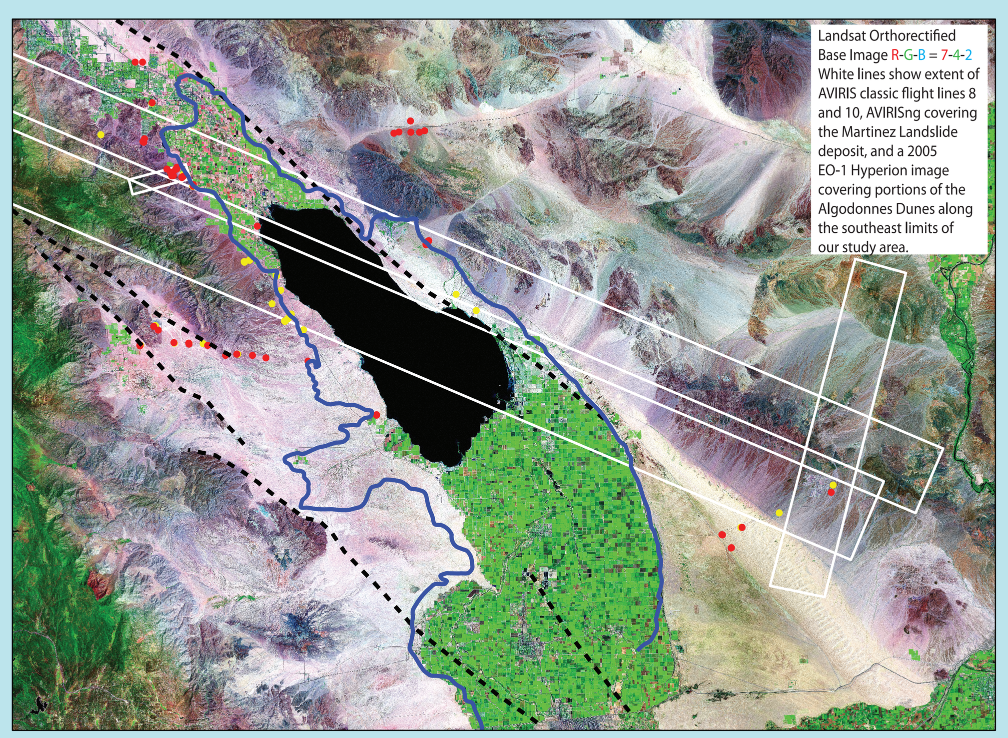

N 0 5 10 20 Kilometers
June 2014 Field Training Sites
August 2013 Field Training Sites
Most recent high shoreline of ancestral Lake Cahuila (~12 masl) (modified and corrected from Norris and Norris, 1961)

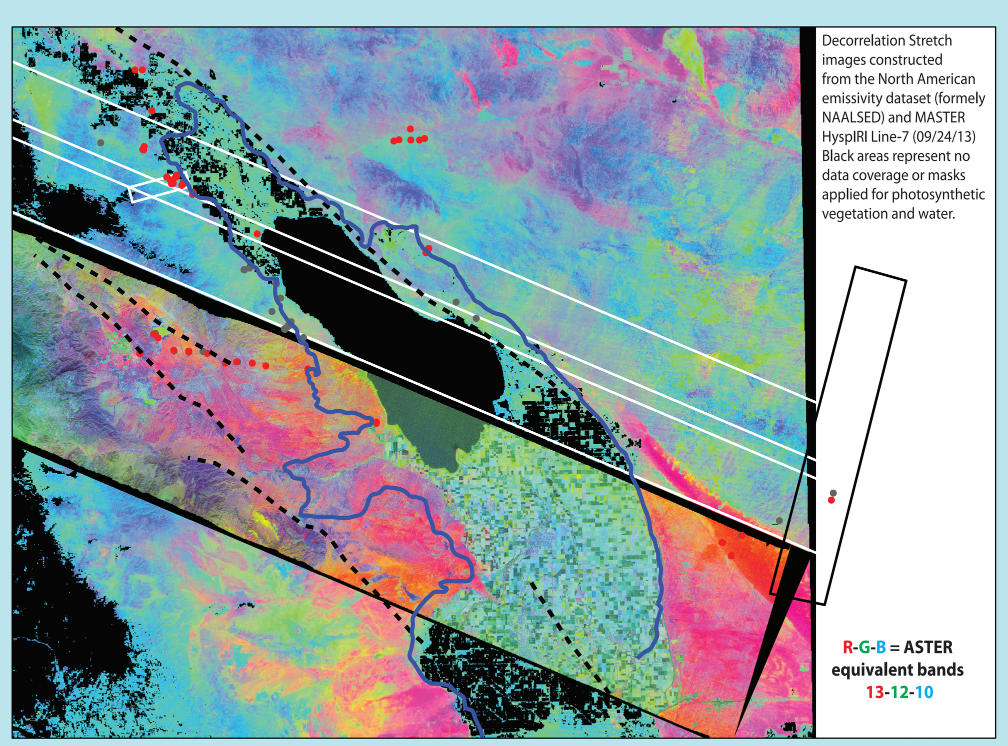

N 0 5 10 20 Kilometers
June 2014 Field Training Sites
August 2013 Field Training Sites
Most recent high shoreline of ancestral Lake Cahuila (~12 masl) (modified and corrected from Norris and Norris, 1961)

The overarching goals of this project is to evaluate HyspIRI-like datasets for mapping minerals that can be used to: 1) understand flood hazards in desert alluvial fan washes, and 2) to discriminate older pavement surfaces from more recently active channels that are more prone to flooding.

We used MICA as a first cut effort at rapid classification of the most dominant minerals in each pixel of AVIRIS-classic, AVIRIS-ng and Hyperion imaging spectrometer data, and subsequent HyspIRI convolved datasets. MICA is loosely based on the Tetracorder algorithm described by Clark et al (2003) and uses continuum-removal, least squares linear regression and analysis of absorption feature band depths to compare observed image spectral features with those from minerals and other substances compiled in spectral libaries (e.g. Clark et al., 2007).

MICA mineral maps helped to guide our fieldwork plans and to select spectral training sites for ASD measurements, calibration and validation purposes, as highlighted in this poster. MICA mineral maps have helped us to: 1) understand the complexity of mixing within alluvial fan bar-n-swale environments and between interacting alluvium, lake and wind-blown sediments; 2) locate spectral endmembers for key minerals indicative of age (e.g. 1-micron desert varnish) and recent flood activity (e.g. 2-micron montmorillonite); 3) gauge the role of rock alteration and related surface processes in understanding potential hazards related to landslides and debris flows; and 4) how to make effective use of accompanying TIR spectral emissivity measurements as shown on the left.

From Clark et al. (2003)

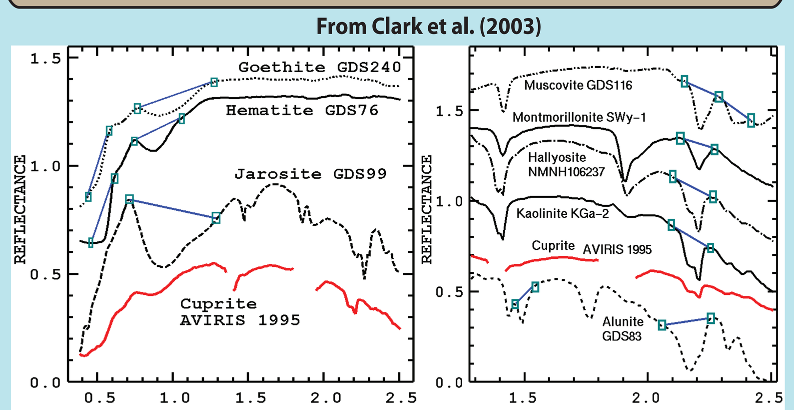

Example Field Calibration Training Site Used for RTGC Correction of Imagery

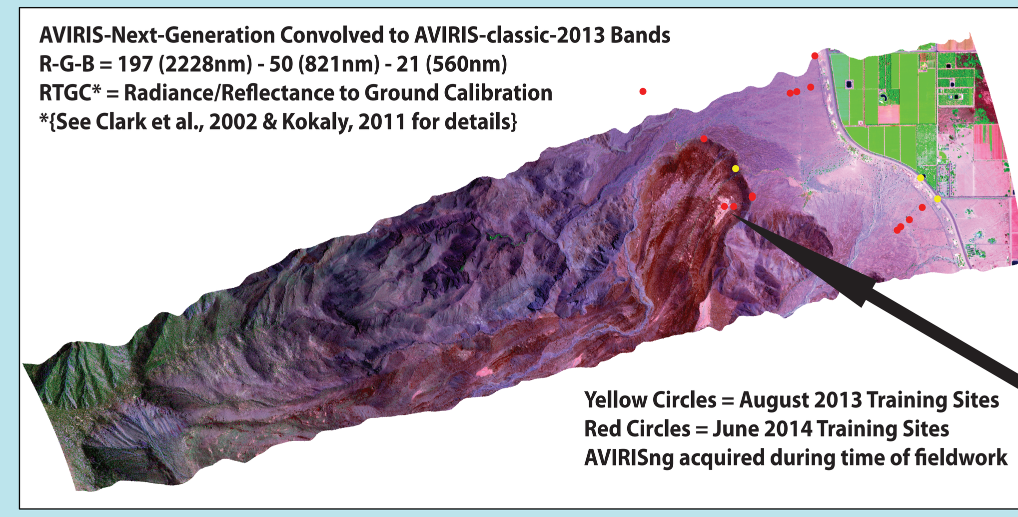

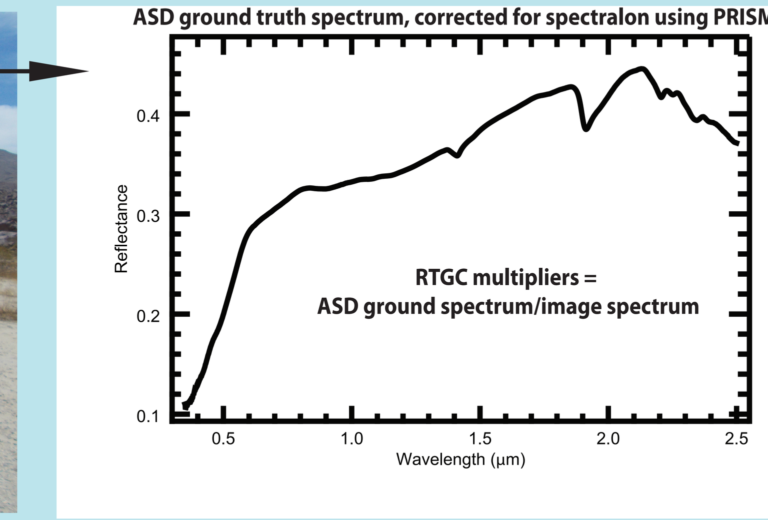

Results-1: AVIRIS-classic MICA mineral maps compared to 60-m HyspIRI-convolved

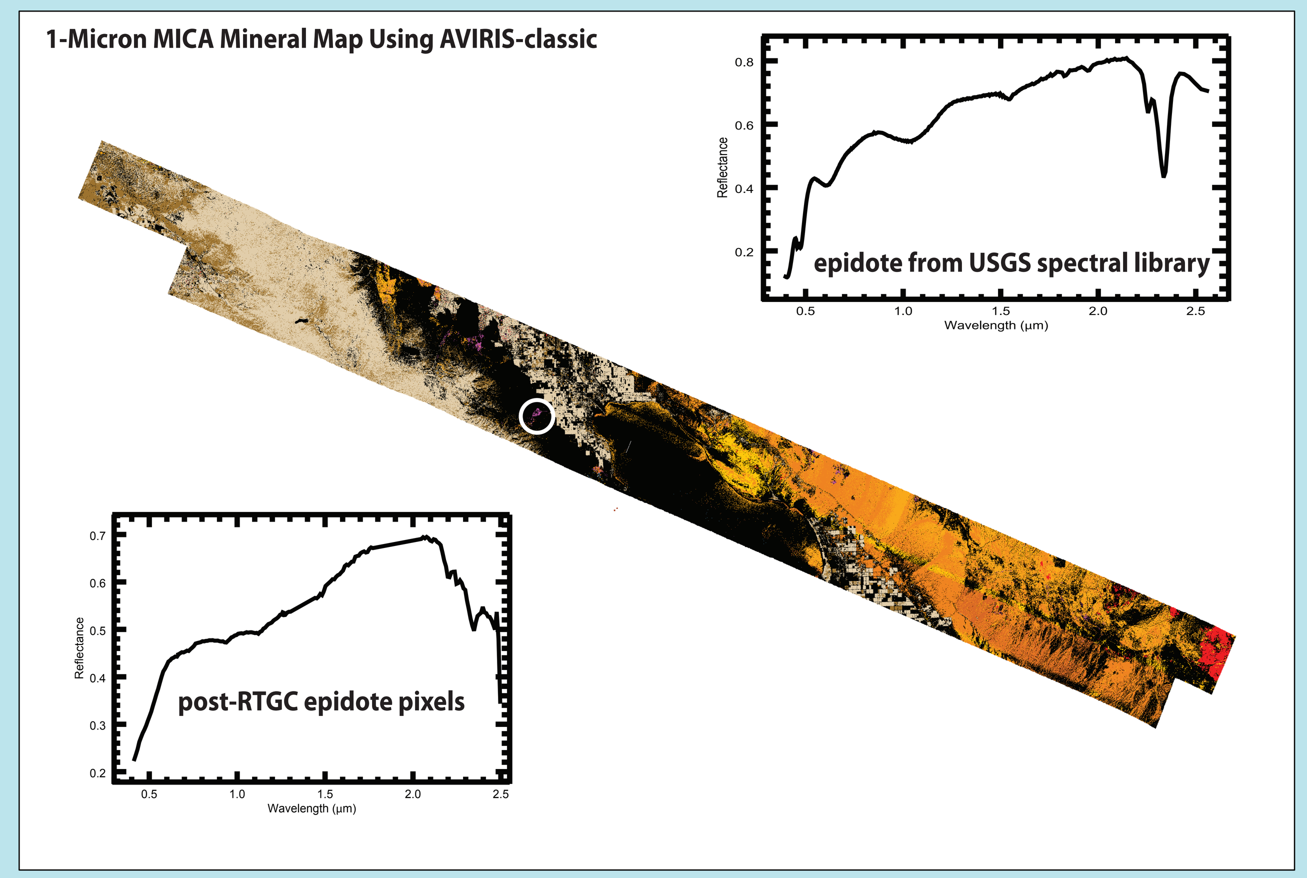

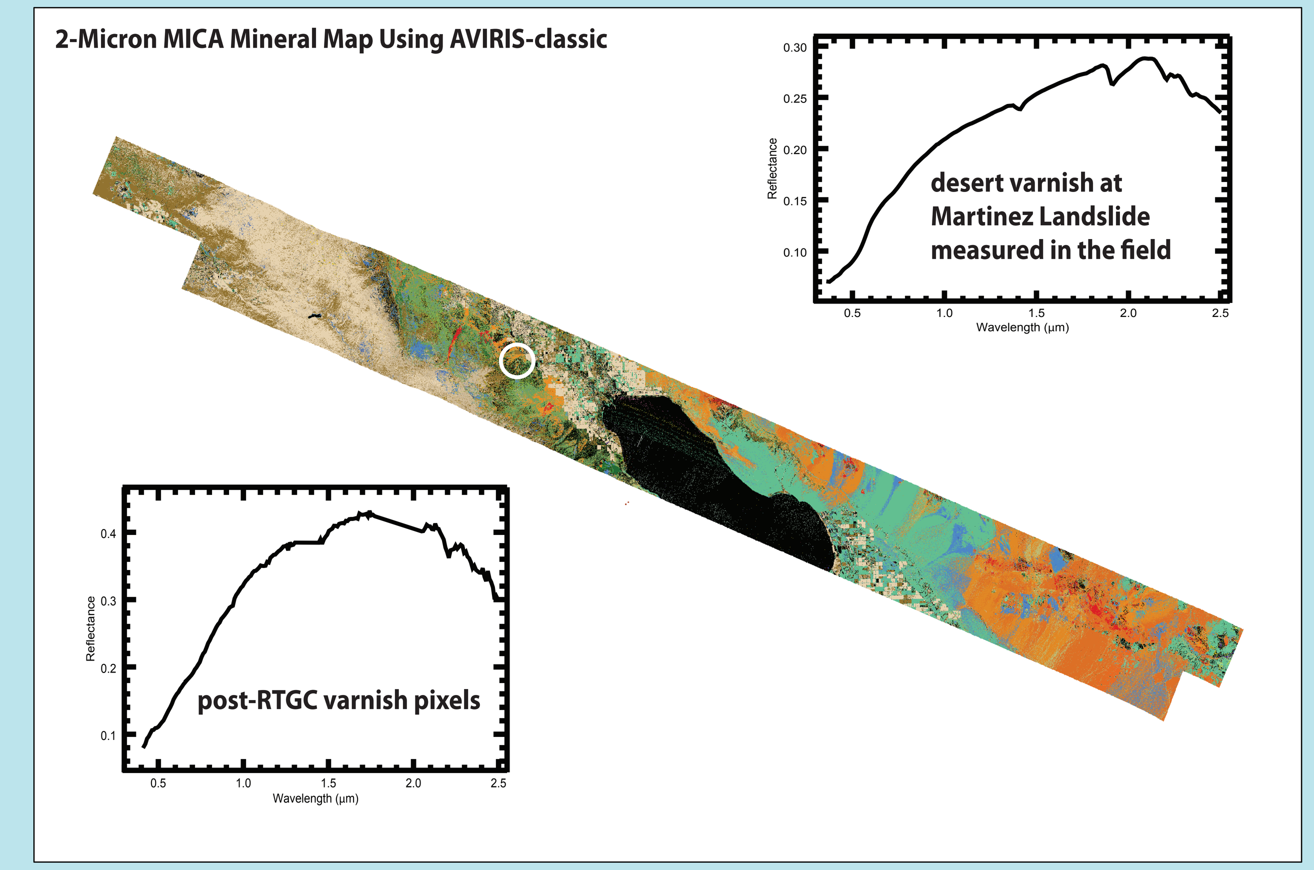

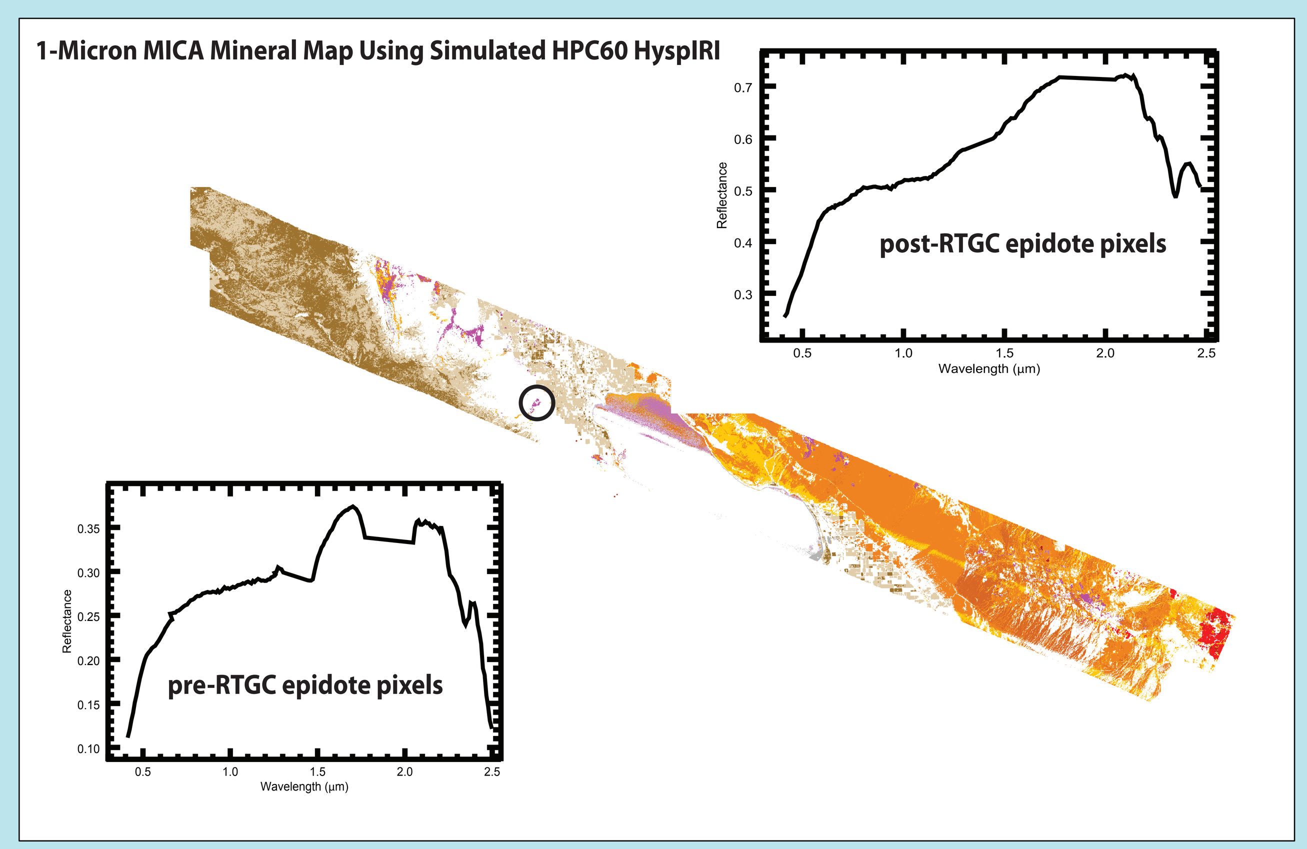

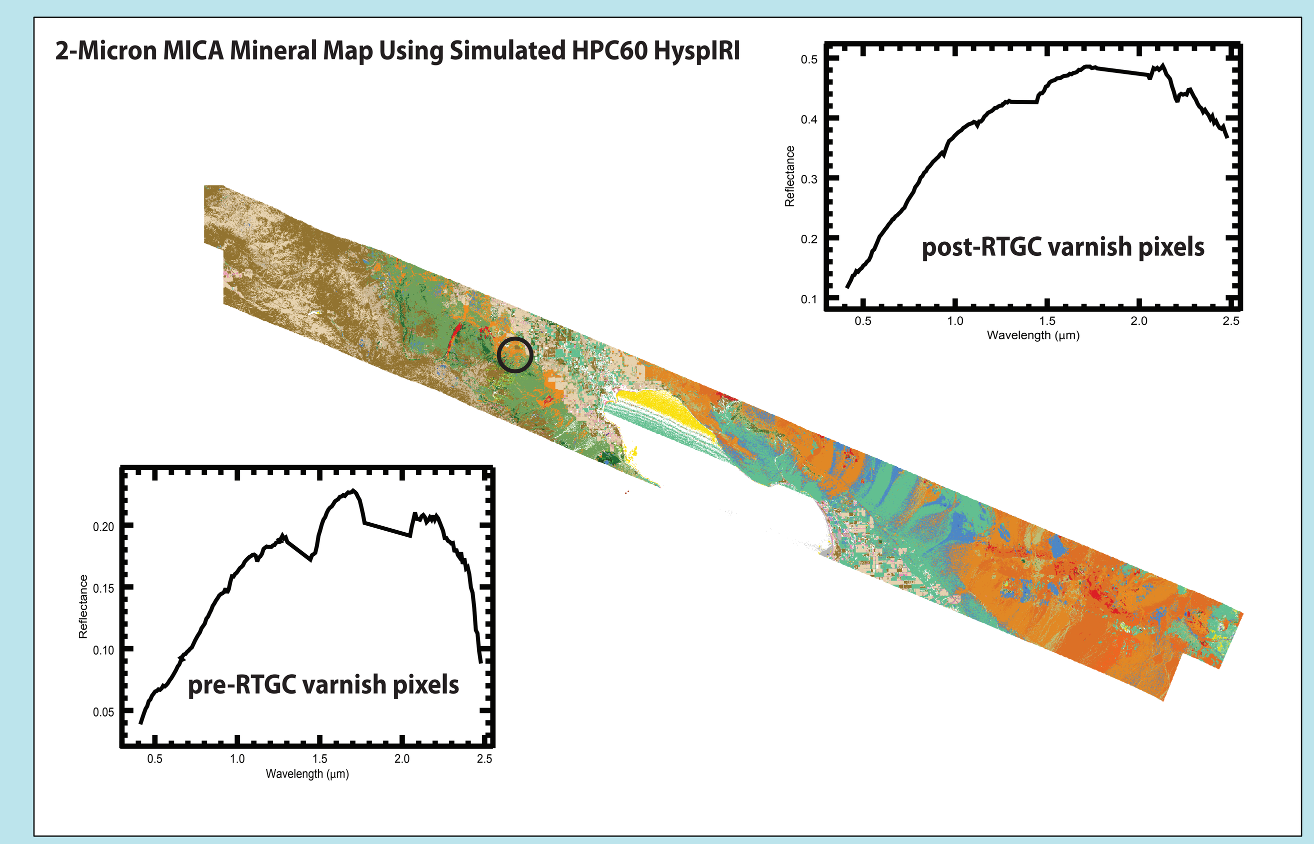

Results-2: How far have we come & where are we going: Hyperion, HyspIRI, AVIRIS-cl, AVIRIS-ng

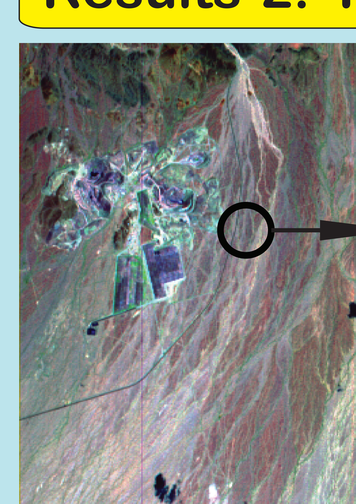

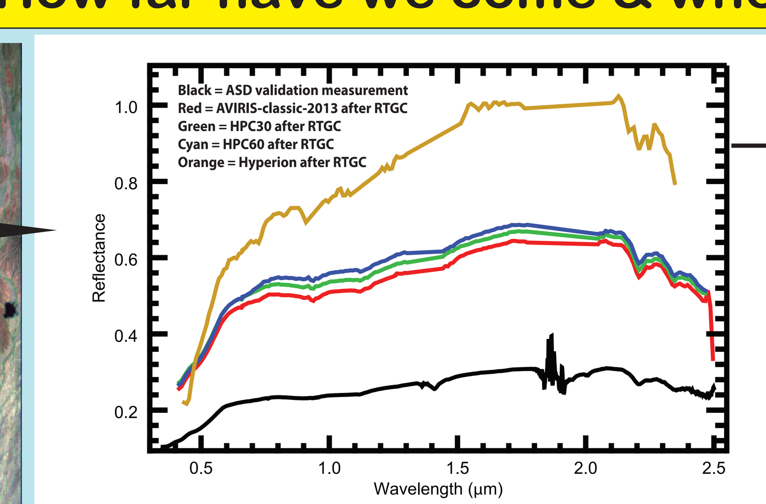

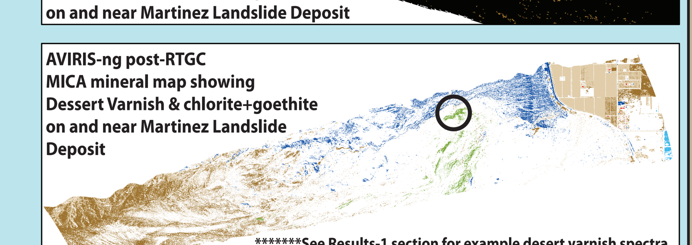

See Results-1 section for example desert varnish spectra dominated by nanocrystalline hematite + Na-montmorillonite

Both Using the same 1-micron MICA command file

MICA Mapping Results Color Legend*

* Based on the command file constructed to produce mineral assessment maps for Afghanistan (see Kokaly et al., 2013) modified for this study by the inclusion of the minerals aragonite and nontronite, as well as a green microline mineral discovered during the course of this study area in parts of the Santa Rosa Mylonite Zone that will be added later.

1-µm thematic map						MICA 1-µm summary image						
Class names in final map	Class value in map	Color in map	Red	Green	Blue	Class names in MICA summary image	Class value in summary image	Color in summary image	Red	Green	Blue	Reference spectrum title
Not classified	0		0	0	0	Not_Classified	0		0	0	0	not applicable
Hematite, nanocrystalline	1		255	0	0	nanohematite.BR34b2	1		255	0	0	Nanohematite BR93-34B2 W1R1Bb
						hematite.thincoat	2		235	0	0	Hematite_Thin_Film GDS27 W1R1Ba
Hematite, fine-grained	2		215	0	0	hematite.finegr.fe2602	3		215	0	0	Hematite FE2602 W1R1Bb
Hematite, medium-grained	3		175	0	0	hematite.medgr.gds27	4		190	0	0	Hematite GDS27 W1R1Ba
						hematite.medgr.br25b	5		175	0	0	Hematite_Coatd_Qtz BR93-25B W1R1Bb
Hematite, coarse-grained	4		140	0	0	hematite.crsegr.br34c	6		155	0	0	Hematite_Coatd_Qtz BR93-34C W1R1Ba
						hematite.crsegr.br25c	7		140	0	0	Hematite_Coatd_Qtz BR93-25C W1R1Bb
Iron hydroxide	5		255	200	0	Fe-hydroxide	8		255	200	0	Fe-Hydroxide SU93-106 amorph W1R1Bb
Goethite, fine-grained	6		255	170	0	goethite.thincoat	9		255	185	0	Goethite_Thin_Film WS222 W1R1Ba
						goethite.finegr.mpcma2b	10		255	170	0	Goethite MPCMA2-B FineGr adj W1R1Bb
Goethite, medium-grained	7		240	130	0	goethite.medgr.ws222	11		240	150	0	Goethite WS222 Medium Gr. W1R1Ba
						goethite.medcrsegr.tracejarosite	15		240	130	0	Goethite MPCMA2-C M-Crsgrad2 W1R1Bb
						goethite+qtz.medgr.gds240	12		240	110	0	Goethite0.02+Quartz GDS240 W1R1Ba
Goethite, coarse-grained	8		215	100	0	goethite.coarsegr.ws222	13		215	100	0	Goethite WS222 Coarse Gr. W1R1Ba
						goethite.coarsegr.gds80	14		215	85	0	Lepidocrosite GDS80 (Syn) W1R1Bb
Goethite and jarosite	9		223	190	255	goethite+jarosite	16		223	190	255	Goeth+qtz.5+Jarosite.5 AMX11 W1R1Bb
Jarosite	10		218	112	214	jarosite.br34a2	17		218	112	214	Jarosite_on_Qtzite BR93-34A2 W1R1Bb
						jarosite_K200	18		208	102	204	Jarosite GDS99 K 200C Syn W1R1Ba
Fe^{2+} type 1	11		0	48	255	Fe2+_type_1a	19		0	48	255	Hypersthene NMNHC2368 W1R1Bb
						Fe2+_type_1b	20		0	38	245	Bronzite HS9.3B Pyroxene W1R1Bc
Fe^{2+} type 2	12		20	132	255	Fe2+_type_2a	21		20	132	255	Cummingtonite HS294.3B W1R1Bc
						Fe2+_type_2b	22		10	122	245	Diopside NMNHR18685 ~160 Pyx W1R1Bb
Fe^{3+} type 1	13		150	230	0	Fe3+_type_1a	23		150	230	0	Schwertmannite BZ93-1 W1R1Bb
						Fe3+_type_1b	24		140	220	0	Acid_Mine_Dr Assemb1-Fe3+ W1R1Fb
						Fe3+_type_1c	25		130	210	0	Acid_Mine_Dr Assemb2-Fe3+ W1R1Fb
Fe^{3+} type 2	14		125	170	0	Fe3+_type_2a	26		125	170	0	Desert_Varnish GDS78A Rhy W1R1Ba

1-µm thematic map						MICA 1-µm summary image						
Class names in final map	Class value in map	Color in map	Red	Green	Blue	Class names in MICA summary image	Class value in summary image	Color in summary image	Red	Green	Blue	Reference spectrum title
						Fe3+_type_2b	27		115	160	0	Desert_Varnish GDS141 W1R1Ba
$Fe^{2+}Fe^{3+}$ type 1	15		0	60	150	Fe2+_Fe3+_type_1	28		0	60	150	Magnetite_skarn BR93-5B W1R1Bb
$Fe^{2+}Fe^{3+}$ type 2	16		0	90	180	Fe2+_Fe3+_type_2a	29		10	100	190	Chlorite+Muscovite CU93-65A W1R1Ba
						Fe2+_Fe3+_type_2b	30		0	90	180	Chlor+Goethite CU93-4B Phyl W1R1Ba
$Fe^{2+}Fe^{3+}$ type 3	17		25	190	255	Fe2+_Fe3+_type_3a	31		45	210	255	Olivine KI3291 Fo29 <60um W1R1Bb
						Fe2+_Fe3+_type_3b	32		35	200	255	Olivine GDS70.c Fo89 70um W1R1Bb
						Fe2+_Fe3+_type_3c	33		25	190	255	Olivine KI3054 Fo66 <60um W1R1Bb
Epidote	18		255	0	255	epidote	34		255	0	255	Epidote GDS26.a 75-200um W1R1Bb
Chlorite	19		199	0	255	chlorite_low_Fe	35		199	0	255	Chlorite SMR-13.b 60-104um W1R1Ba
						chlorite_high_Fe	36		189	0	245	Thuringite SMR-15.c 32um W1R1Ba
Maghemite	20		171	122	255	maghemite	37		171	122	255	Maghemite GDS81 Syn (M-3) W1R1Bb
Ferrihydrite	21		255	255	0	ferrihydrite	38		255	255	0	Ferrihydrite GDS75 Syn, F6 W1R1Bb
Green vegetation	22		225	205	170	vegetation1	39		225	205	170	Fir_Tree IH91-2 W1R1Ba
						vegetation.dry+green	40		220	200	165	Grass_dry.7+.3green AMX30 W1R1Ba
Dry vegetation	23		157	115	48	dry_veg_grass	41		162	120	53	Grass_Golden_Dry GDS480 W1R1Fa
						dry_veg_grass_2_3um	42		157	115	48	Grass_Golden_Dry GDS480 W1R1Fa
						dry_veg_nongrass	43		137	105	38	Lodgepole-Pine LP-Needles-3 W1R1Fa
						dry_veg_nongrass_2_3um	44		132	100	33	Lodgepole-Pine LP-Needles-3 W1R1Fa
Snow and ice	24		80	0	115	snow_melting	45		80	0	115	Melting_snow mSnw1a W1R1Fa
						snow_slush	46		75	0	110	Melting_snow mSnw9 (slush) W1R1Fa
Water	25		180	180	180	water	47		180	180	180	Seawater_Coast_Chl SW1 W1R1Ba
						water_sediment_low	48		175	175	175	Water+Montmor SWy-2+0.5g/l W1R1Fa
						water_sediment_high	49		170	170	170	Water+Montmor SWy-2+5.01g/l W1R1Fa
Wet soils*	26		140	140	140	Wet-Soil*	50		140	140	140	not applicable
No data	27		60	60	60	Nondata Pixel	51		60	60	60	not applicable
Cloud or cloud shadow	28		225	225	225	Cloud	52		255	255	255	not applicable

2-µm thematic map						MICA 2-µm summary image						
Class names in final map	Class value in map	Color in map	Red	Green	Blue	Class names in MICA summary images	Class value in summary image	Color in summary image	Red	Green	Blue	Reference spectrum title
Not classified	0		0	0	0	not classified (image_unmapped_pixels)	0		0	0	0	not applicable
Calcite, abundant	1		20	75	0	calcite_abundant	1		20	75	0	Calcite WS272 W1R1Ba
Calcite	2		40	105	10	calcite	2		40	105	10	Calcite WS272 W1R1Ba
Calcite and muscovite/clay	3		113	160	90	calcite.7+muscovite.3	3		113	160	90	Calcite+.33Muscov AMX5 Ruby W1R1Ba
Calcite and clay/muscovite	4		188	185	115	calcite.8+montmorillonite_Ca.2	4		188	185	115	Calcite.8+Ca-Montmor.2 AMX15 W1R1Bb
						calcite.8+montmorillonite_Na.2	5		178	175	105	Calcite.80+Mont_Swy-1 GDS212 W1R1Ba
Carbonate and clay/muscovite	5		135	155	60	dolomite.25+calcite.25+mont_Na.5	9		135	155	60	Calc.25+dolo.25+mont.5 AMX18 W1R1Bb
Carbonate, iron-bearing	6		220	185	255	carbonate_Fe_bearing	6		220	185	255	Siderite HS271.3B W1R1Ba
Dolomite	7		205	25	255	dolomite	7		205	25	255	Dolomite HS102.3B W1R1Bb
Dolomite and clay/muscovite	8		165	20	200	dolomite.5+montmorillonite_Na.5	8		165	20	200	Dolomite.5+Na-mont.5 AMX21 W1R1Bb
Epidote or chlorite	9		225	25	0	epidote	10		215	15	0	Epidote GDS26.a 75-200um W1R1Bb
						chlorite_lowFe	11		225	25	0	Chlorite SMR-13.b 60-104um W1R1Ba
						chlorite+muscovite	12		245	45	20	Chlorite+Muscovite CU93-65A W1R1Ba
Muscovite	10		250	150	0	muscovite_lowAl	13		255	155	5	Muscovite CU93-1 low-Al Phyl W2R4Nb
						muscovite_medAl	14		250	150	0	Muscovite-medlowAl CU91-250A W1R1Fb
						muscovite_medhighAl	15		245	145	0	Muscovite GDS113 Ruby W1R1Bb
						muscovite_Fe-rich	16		240	140	0	Muscovite GDS116 Tanzania W1R1Ba
Illite	11		230	120	0	illite	17		230	120	0	Illite IMt-1.b <2um W1R1Ba
						illite_gds4	18		220	110	0	Illite GDS4 (Marblehead) W1R1Bb
Kaolinite (alunite, pyrophyllite or dickite may be present)	12		30	30	185	alunite.25+kaolinite.75	32		35	35	190	Kaolwxl.75+Alun_HS295 AMX14 W1R1Bb
						pyrophyllite+kaolinite	35		30	30	185	Pyrophyl.25+wxlKaol.75 AMX17 W1R1Bb
						kaol_possible_alunite_or_dickite	39		25	25	180	Dickite NMNH106242 W1R1Bb
Kaolinite	13		25	85	245	kaolinite_wxl	19		10	70	230	Kaolinite CM9 W1R1Bb
						kaolinite_pxl	20		25	85	245	Kaolinite KGa-2 (pxl) W1R1Bb
Kaolinite and muscovite/ clay/carbonate	14		40	145	255	kaolin+clay_mica_or_halloysite	21		25	130	240	Halloysite NMNH106237 W1R1Ba
						kaolin.5+muscovite_medAl	22		30	135	245	Kaol.5+MuscCU91-250A AMX13 W1R1Bb
						kaolin+muscovite_mix_intimate	23		35	140	250	Kaol+Musc_intimate CU93-5C W1R1Ba
						kaolin.5+muscovite_medhighAl	24		40	145	255	Kaol_Wxl+0.5Musc_Ruby AMX12 W1R1Ba
						kaolin.5+smectite.5	25		45	150	255	Kaolin_Smect H89-FR-2 .5Kaol W1R1Bb
						kaolin.2+calcite.8	26		50	155	255	Calcite.80wt+Kaol_CM9 GDS213 W1R1Ba
Montmorillonite	15		130	210	255	montmorillonite_Na	27		130	210	255	Montmorillonite SWy-1 W1R1Bb
						montmorillonite_Ca	28		125	205	250	Montmorillonite SAz-1 W1R1Bb
Alunite	16		250	160	185	alunite_Na_450c	29		250	160	185	Alunite RES-3 Na Syn (450C) W2R4Na
						alunite_K_250c	30		245	155	180	Alunite GDS96 K Syn (250C) W2R4Na
Alunite and kaolinite	17		255	195	195	alunite.5+kaolinite.5	31		255	195	195	Alunite0.5+Kaol_KGa-1 AMX3 W1R1Bb

2-µm thematic map						MICA 2-µm summary image						
Class names in final map	Class value in map	Color in map	Red	Green	Blue	Class names in MICA summary images	Class value in summary image	Color in summary image	Red	Green	Blue	Reference spectrum title
Pyrophyllite (alunite or kaolinite may be present)	18		145	25	55	pyrophyllite	33		145	25	55	Pyrophyllite PYS1A fine gr W1R1Ba
						pyrophyllite.5+alunite.5	34		155	35	65	Alunite+Pyrophyl SD1093A W1R1Bb
Jarosite	19		218	112	214	jarosite_Na	36		218	112	214	Jarosite GDS24 Na W1R1Bb
						jarosite_K	37		213	107	209	Jarosite GDS99 K 200C Syn W1R1Ba
						jarosite+muscovite_mix_intimate	38		208	102	204	Muscov+Jaros CU93-314 coatng W1R1Bb
Buddingtonite	20		255	210	0	buddingtonite	40		255	210	0	Buddingtonite GDS85 D-206 W1R1Bb
						buddingtonite+montmorillonite	41		245	200	0	Buddingtnt+Na-Mont CU93-260B W2R4Nb
Serpentine	21		160	215	50	serpentine1	42		160	215	50	Chrysotile HS323.1B W1R1Ba
						serpentine2	43		155	210	45	Antigorite NMNH96917.d 70um W1R1Bb
						serpentine3	44		150	205	40	Chrysotile HS323.1B W1R1Ba
						serpentine4	45		145	200	35	Antigorite NMNH96917.d 70um W1R1Bb
Serpentine, or dolomite and calcite	22		176	131	255	serpentine_or_dolomite+calcite	46		176	131	255	Antigorite NMNH96917.d 70um W1R1Bb
Tremolite or talc	23		100	40	180	tremolite_or_talc	47		100	40	180	Tremolite HS18.3 W1R1Bc
Hydrated silica	24		255	255	75	hydrated_silica	48		255	255	75	Opal TM8896 (Hyalite) W1R1Ba
						chalcedony	49		250	250	70	Chalcedony CU91-6A W1R1Ba
Gypsum	25		240	0	255	gypsum	50		240	0	255	Gypsum HS333.3B (Selenite) W1R1Ba
Green vegetation	26		225	205	170	vegetation_green	51		225	205	170	Fir_Tree IH91-2 W1R1Ba
						vegetation.dry+green	52		220	200	165	Grass_dry.7+.3green AMX30 W1R1Ba
Dry vegetation	27		157	115	48	dry_veg_grass	53		162	120	53	Grass_Golden_Dry GDS480 W1R1Fa
						dry_veg_grass_2_3um	54		157	115	48	Grass_Golden_Dry GDS480 W1R1Fa
						dry_veg_nongrass	55		137	105	38	Lodgepole-Pine LP-Needles-3 W1R1Fa
						dry_veg_nongrass_2_3um	56		132	100	33	Lodgepole-Pine LP-Needles-3 W1R1Fa
Snow and ice	28		80	0	115	snow_melting	57		80	0	115	Melting_snow mSnw1a W1R1Fa
						snow_slush	58		75	0	110	Melting_snow mSnw9 (slush) W1R1Fa
Water	29		180	180	180	water	59		180	180	180	Seawater_Coast_Chl SW1 W1R1Ba
						water_sediment_low	60		175	175	175	Water+Montmor SWy-2+5.01g/l W1R1Fa
						water_sediment_high	61		170	170	170	Water+Montmor SWy-2+0.5g/l W1R1Fa
Wet soils*	30		140	140	140	Wet-soil*	62		140	140	140	not applicable
No data	31		60	60	60	Non-data pixel	63		60	60	60	not applicable
Cloud or cloud shadow	32		225	225	225	Cloud	64		255	255	255	not applicable

References Cited

Clark, R.N., Swayze, G.A., Livo, K.E., Kokaly, R.F., King, T.V.V., Dalton, J.B., Vance, J.S., Rockwell, B.W., Hoefen, T., and McDougal, R.R., 2002, Surface reflectance calibration of terrestrial imaging spectroscopy data: A tutorial using AVIRIS, in Proceedings of the 10th Airborne Earth Science Workshop, JPL Publication 02-1.

Clark, R.N., Swayze, G.A., Livo, K.E., Kokaly, R.F., Sutley, S.J., Dalton, J.B., and others, 2003, Imaging spectroscopy: Earth and planetary remote sensing with the USGS Tetracorder and expert systems: Journal of Geophysical Research, v. 108(E12), p. 5131–5146.

Clark, R.N., Swayze, G.A., Wise, R., Livo, E., Hoefen, T., Kokaly, R., and Sutley, S.J., 2007, USGS digital spectral library splib06a: U.S. Geological Survey Digital Data Series 231, available online at http://speclab.cr.usgs.gov/spectral.lib06.

Kokaly, R.F., 2011, PRISM: Processing routines in IDL for spectroscopic measurements (installation manual and user's guide, version 1.0): U.S. Geological Survey Open-File Report 2011–1155, 432 p.

Kokaly, R.F., King, T.V.V., and Hoefen, T.M., 2013, Surface mineral maps of Afghanistan derived from HyMap imaging spectrometer data, version 2: U.S. Geological Survey Data Series 787, 29 p., http://pubs.usgs.gov/ds/787/.

Version 2 March15, 2013 BDS